Applied Surface Science 513 (2020) 145721

Contents lists available at ScienceDirect

Applied Surface Science

journal homepage: www.elsevier.com/locate/apsusc

Full Length Article

Property engineering through nanomaterial chemical transformation of colloidal nanocrystal thin films

Md Ashraf Hossain[a], Sanghyun Jeon[a], Junhyuk Ahn[a], Junsung Bang[a], Ho Kun Woo[a], Shihab B. Hafiz[b], Dong-Kyun Ko[b,*], Soong Ju Oh[a,*]

[a] Department of Materials Science and Engineering, Korea University, Seoul 02841, Republic of Korea
[b] Department of Electrical and Computer Engineering, New Jersey Institute of Technology, Newark, NJ 07102, United States

ARTICLE INFO

Keywords:
Silver selenide
Chemical transformation
Metal chalcogenides
N-type semiconductor
Transport

ABSTRACT

Herein, we introduce a unique nanomaterial chemical transformation (NCT) process whereby selenium (Se) anion is introduced to colloidal silver (Ag) nanocrystals (NCs) to create nanostructured silver selenide (Ag_2Se). We present a complete suite of material characterizations, including chemical, structural, optical, and electrical characterizations to understand the details of the transformation process. The Ag_2Se thin-films obtained through the NCT process exhibit degenerately-doped n-type semiconductor characteristics with high carrier mobility. We discuss the chemical mechanism that drives the material transformation and elucidates the origin of doping in these semiconducting thin-films. We also demonstrate the robustness of Ag_2Se thin-films toward mechanical strain and temperature cycling stress for flexible device applications. We believed that the NCT process demonstrated here is of wide applicability to other material systems which can open up new avenues for solid-state chemistry and device engineering research.

1. Introduction

Nanomaterial chemical transformation (NCT) has recently emerged as a powerful materials tool to engineer chemical, structural, and morphological properties down at the nanoscale. Utilizing the advantage of large surface to volume ratio and chemically-active surface area of the host nanomaterial, chemical transformation takes place via substitution or inclusion of foreign atoms inside the parent material system. To date, a number of different NCT approaches, including ion exchange, surface treatment and galvanic replacement processes [1–6], have been demonstrated with promising prospects for solar cell [7–10]. energy storage [11–14], sensor [15–18], electrocatalyst [19–21], optoelectronic [22–25], and biomedical device [26–28] applications. In particular, ion exchange method has been the highlight of NCT due to its high degree of thermodynamic and kinetic control over the final product, enabling the preparation of precise heterostructures [29], core-shell structures [29–32] and even metastable phases [33,34] that are typically inaccessible using conventional synthetic chemistry. In this method, both cation and anion exchange is possible, as exemplified by the diverse materials library created through ionic transformation: CdSe to Cu_2Se to ZnSe [34], Al_2O_3 to AlN [35] ZnS to ZnO [36], and CoO to Co_3S_4 [37,38].

Silver selenide (Ag_2Se) is a rarely explored member of the metal chalcogenide family that exhibits unique structural and electronic characteristics [39]. At low temperature, Ag_2Se is a narrow band-gap semiconductor (0.07–0.15 eV) while the high-temperature phase is known to exhibit high ionic conductivity with potential applications range from thermoelectrics [40], infrared detectors [41–44], to CO_2 reduction [45,46]. In particular, nanostructured Ag_2Se have been in spotlight as they exhibit unique intraband optical transitions, which can be utilized to spur new applications. Typically, nanostructured Ag_2Se have been synthesized using sonochemical methods [47], vapor-phase growth [48], and high temperature and high-pressure solution-phase reactions [48,49], These processes typically require high temperature and high vacuum conditions, long reaction time, or involve the use of expensive techniques, otherwise they produce polycrystalline and polydisperse Ag_2Se nanocrystals. The colloidal synthesis of nanosized Ag_2Se is an alternate route to obtaining nearly monodisperse, nanometer-sized Ag_2Se. The chemical transformation of metal chalcogenide NC into Ag_2Se have also been investigated previously [50,51]. However, the synthetic yield of Ag_2Se is low and the films prepared using these NCs exhibit inferior electrical properties since the NC surface are covered with long, insulating hydrocarbon ligands that hinders charge transport between NCs.

* Corresponding authors.
E-mail addresses: dkko@njit.edu (D.-K. Ko), sjoh1982@korea.ac.kr (S.J. Oh).

https://doi.org/10.1016/j.apsusc.2020.145721
Received 14 November 2019; Received in revised form 23 January 2020; Accepted 9 February 2020
Available online 10 February 2020
0169-4332/

In this work, we present a unique NCT route whereby selenium (Se) anion is introduced to a colloidal metallic silver (Ag) nanocrystals (NCs) to induce chemical transformation to semiconducting silver selenide (Ag_2Se) nanostructured thin films. Unlike previous attempts that involve colloidal chemical transformation, our NCT enables the transformation of a large area, solid-state thin film to engineer materials with new physical properties. Also, our process is based on facile solution processing which is amenable to a large area, high-throughput fabrication. The NCT presented here is accompanied by a property transformation from metallic to semiconducting (degenerate) state. We eluciate the mechanism of the chemical transformation process and examine the temporal evolution of metallic-to-semiconducting property transition through combined chemical, structural, optical, and electrical characterizations. In addition, we demonstrate that our NCT-derived Ag_2Se thin films are insensitive to externally applied mechanical and thermal stresses which are advantageous for flexible electronics applications. We believe that the detailed insights gained from this work can serve as a foundation for extending to other material systems and new application in thermoeletrics and infrared optoelectronics or optics such as infrared detector or zero-energy cooling system for solid-state chemists and device engineers.

2. Experimental

2.1. Materials

Sodium selenide (Na_2Se, 99.8%), silver nitrate ($AgNO_3$, 99%), and n-octane (98 + %) were bought from Alfa Aesar Co., Inc. Oleylamine (OAm, 70%), oleic acid (OA, 90%), hexane (99%), methanol (99.8%) and (3-mercaptopropyl) trimethoxysilane (MPTS, 95%), were bought from Sigma Aldrich Co., Ltd. 250 μm thick PET (Polyethylene terephthalate) films were bought from SK films that used as flexible substrates in this study.

2.2. Synthesis of silver nanocrystals (Ag NCs)

Ag NCs synthesis process of this study was adopted from earlier reports with little modification [52]. 3.5 g of $AgNO_3$ powder, 90 mL of OA, and 6 mL of OAm solution were mixed by magnetic stirring in a round bottom three-neck flask. This solution was heated up to 343 K and degassed under the vacuum for 90 min. After the degassing process, the solution temperature was elevated to 453 K at a heating rate of 3 K per 3 min. After that, the solution was allowed to cool to ambient temperature. The as-synthesized Ag NCs were obtained by washing through the centrifugation process adding toluene and ethanol. This washing process was repeated three to five times. Finally, Ag NCs were dispersed in n-octane or hexane at various concentrations such as 50 to 200 mg mL^{-1}.

2.3. Preparation of substrate

For this study purpose, all substrates (PET, silicon wafer, glass) were sequentially washed by acetone, *iso*-propyl alcohol, and de-ionized (DI) water in the sonication bath. After that, all substrates were treated with UV-ozone. for 30 min. Finally, the substrates were immersed in a solution of 5% (vol.) MPTS to produce a self-assembled monolayer (SAM) on the substrate which enhancing adhesion between Ag NCs and substrate.

2.4. Fabrication and chemical treatment of Ag NCs thin films

In order to fabricate Ag NCs thin films, the as-synthesized Ag NCs were spin-coated on a pre-treated substrate at a speed of 1000 rpm for 30 s. The 10 mM Na_2Se solution was prepared in methanol. The as-fabricated Ag NCs thin films were treated with 10 mM Na_2Se solution for 30 s to 180 s. After that, thin-films were washed by methanol several times to exclude the excess Na_2Se solution from the surface.

2.5. Characterization

Surface morphologies of Ag NCs thin-films and chemical treated Ag_2Se thin-films were characterized by scanning electronic microscopy energy-dispersive X-ray (SEM-EDX, Hitachi S-4300, Hitachi High technologies America, Inc.) and transmission electron microscopy (TEM, Tecnai 20, ThermoFisher Scientific). Their structural properties were characterized by X-ray diffraction spectroscopy (XRD, MAX-2500V, Rigaku). The optical and chemical properties were characterized by UV–vis spectroscopy (Cary 5000, Agilent Technologies) and FT-IR spectroscopy (LabRam ARAMIS IR2, Horiba Jobin Yvon). The electromechanical properties of samples were characterized by a probe station (MST 4000, MS Tech). The resistivity and sheet resistance of samples were measured by a four-point probe (CMT-SR2000N, Materials Development Corporation). Carrier concentration and mobility were measured by Hall effect measurement system (H-5000, MMR Technologies) with 0.5 T fixed magnet using standard van der Pauw configuration.

3. Result and discussion

The overall process of transformation is illustrated in Fig. 1. Prior to the transformation process, Ag NCs were prepared following the previously reported colloidal synthesis procedure [52]. The Ag NCs were then spin-coated on the MPTS-treated substrate to form a thin-film. The as-deposited Ag NCs thin films were electrically insulating because the long organic ligands (oleic acid and olelyamine) that coat the NCs surface prohibit charge transport between NCs. We developed a chemical transformation process, namely Na_2Se solution treatment, that simultaneously remove the organic long insulating ligands and transform Ag NCs into Ag_2Se thin films in a single step. We conduct this treatment with varying durations (0, 30 and 180 s) to investigate temporal changes in chemical, structural, optical, and electrical properties.

To verify the transformation process, FT-IR spectroscopy analysis was conducted to investigate the surface chemistry of the Ag NCs thin-film before and after treated with Na_2Se, as shown in Fig. 2a. Before Na_2Se treatment, a strong C—H vibration peak around 3000 cm^{-1} was observed, which arises from organic capping ligands of Ag NCs. Upon treatment of Na_2Se solution for 30 s, the C—H vibration peak intensity was significantly reduced, indicating that oleic acid and oleylamine were partially removed during this treatment. The ligand removal was complete after 180 s, as evidenced by the disappearance of C—H vibrational peak. Furthermore, energy dispersive X-ray (EDX) spectroscopy analysis was conducted to investigate the chemical composition change, which is shown in Fig. 2b, 2c and Figure S1 in the supporting information. The quantity of Se in Ag NCs thin-film increased from 0% to 30% after 30 s of Na_2S treatment and was further increased to 47% up to 180 s of treatment time. At the treatment time of 180 s, the stoichiometric ratio of selenium and silver was close to 2:1. The mechanism of Ag_2Se thin-film formation by chemical transformation process can be described as follows:

$$n(Ag - oleate) + Na_2Se \rightarrow Ag_2Se + n(Na - oleate)$$

To further confirm that Se is incorporated inside the crystal lattice and not on the NC surface, X-ray diffraction (XRD) analysis was performed (Fig. 2d). Before Na_2Se treatment, the as-synthesized Ag NCs exhibit a Scherrer-broadened diffraction peak at 39.31° that corresponds to a (1 1 1) plane of a Ag crystal. After 30 s of Na_2Se treatment, new diffraction peaks of Ag_2Se at 22.99, 26.84, 31.00, 32.86, 33.58, 34.85, 37.02, 40.21, 42.82, 43.53, 45.19, 48.63°, which correspond to the (0 0 2), (1 1 1), (1 0 2), (1 2 0), (1 1 2), (1 2 1), (0 1 3), (1 2 2), (1 1 3), (0 2 3), (2 1 1) and (0 1 4) planes, respectively, emerge. The diffraction pattern coincides with JCPDS-241041 data of orthorhombic

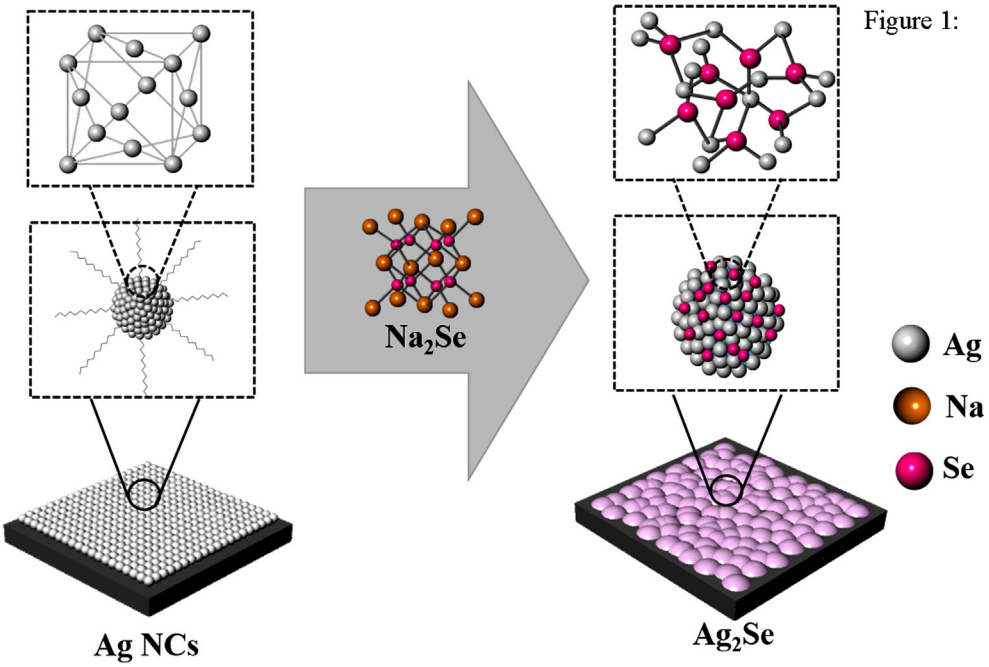

Fig. 1. Schematic illustration of nanomaterials chemical transformation of Ag NCs to Ag_2Se thin-film.

Ag_2Se. Notably, the intensity of silver peak at 39.31° was reduced at a treatment time of 30 s and was entirely disappeared at 180 s Na_2Se treatment time, implying the successful chemical transformation of Ag into Ag_2Se films. These Ag_2Se peaks emerge and become strongly pronounced at a treatment time of 180 s. The sharpening of the XRD peak (from 30 s to 180 s) observed here indicates that the chemical and structural transformation is accompanied by morphological changes.

The formation of Ag_2Se was further confirmed through the photoelectron spectroscopy (XPS) analysis. The survey spectrum suggested the presence of Ag and Se in the sample thin-films (see supporting information Figure S2). As shown in Fig. 2e, an expanded region of silver show Ag $3d_{5/2}$ binding energy at 367.1 eV and Ag $3d_{3/2}$ binding energy at 373.1 eV [53], which indicate the oxidation of Ag ions in the univalent state. The peak at 53.2 eV in Fig. 2f corresponds to Se 3d [53].

To examine the detailed morphology of transformed films, we conducted a high-resolution transmission electron microscopy (HRTEM). Initially, as-synthesized Ag NCs exhibited uniform size and spherical shape with an average nanocrystal size of (4.7 ± 0.14) nm which is shown in Fig. 3a. Upon exposure to Na_2Se solution for 30 s which shown in Fig. 3b, a significant NC fusion takes place as the bulky organic ligands are detached from the surface thereby facilitating facile ionic movement between NCs and concurrently, the short inorganic Se^{2-} ion was attached on the NCs. After 180 s of treatment time, the Ag NCs sintered together as large Ag NCs with selenium elements bound to nonspecific directions. As a result, NC clusters became irregular in size and uneven in shape which is present in Fig. 3c. On the other hand, scanning electron microscopy (SEM) analysis to examine the film uniformity. Prior to the Na_2Se treatment, Ag NCs were evenly dispersed on the substrate surface without any holes and cracks. After the treatment with Na_2Se for 30 s and 180 s, a uniform, continuous film consisting of an assembly of homogeneous NCs were transformed into a non-uniform, nanoporous film made from randomly fused NCs, as shown in Fig. 3a to 3c.

The transformation from metal Ag to semiconducting Ag_2Se observed here should directly translate into the changes in the optical property. We carry out optical absorption measurement in the UV to visible range on Ag NCs films before and after the Na_2Se treatment, as shown in Fig. 3c. As-synthesized Ag NCs thin-film showed a distinct localized surface plasmon resonance (LSPR) peak at around 440 nm and this is in agreement with the previous report [54]. After the Na_2Se treatment, this LSPR peak is red-shifted, quenched, and broadened. The observed red-shift can be understood in terms of reduction in carrier concentration as the material transforms from metal to semiconductor [55]. The intensity quenching and peak broadening are expected to arise from irregular NC fusion that results in a large distribution of size and shapes of plasmonic resonators.

In order to understand the electrical properties of Ag NCs and Na_2Se treated Ag_2Se thin-films, current-voltage (*I-V*) characteristics were measured, as shown in Fig. 4a. The Ag NCs thin-film showed extremely high electrical resistance, outside the range of our measurement system, hence *I-V* data could not be obtained. However, after 30 s of Na_2Se treatment, a linear *I-V* curve was obtained, the corresponding total electrical resistivity of $(1.65 \pm 0.06) \times 10^{-3}$ Ω·cm. The film resistivity showed a decreasing trend with increasing treatment time. The resistivity of $(2.00 \pm 0.01) \times 10^{-4}$ Ω·cm was measured from the film with 180 s of treatment. While the treatment induces a transformation from metallic to semiconducting state with decreasing carrier concentration, the resistivity trend observed here suggest that the reduction in carrier concentration is small and the change in the carrier mobility is the dominant factor that determines the electrical resistivity of the film. Hall effect measurements result obtained from Na_2Se treated Ag_2Se film indicate a high electron concentration of $(5.7 \pm 2) \times 10^{19}$ cm^{-3}, making the film a degenerate semiconductor, in alignment with the discussion above. The Hall mobility was measured to be (30.6 ± 8) $cm^2\ V^{-1}\ s^{-1}$, which is a magnitude well above the range expected for a material exhibiting hopping transport (typical hopping mobility: 0.001–1 $cm^2\ V^{-1}\ s^{-1}$). The Na_2Se treatment brings reduction in inter-NC spacing due to ligand stripping and ultimately leads to NC fusion that create continuous paths for carriers to transport with high mobility. We conducted a temperature-dependent electrical resistance measurements to further examine the detailed carrier transport property. Fig. 4b shows that data obtained from a film treated with 180 s of Na_2Se. Typical NC film is characterized by thermally-activated hopping transport [56]. Under this transport mechanism, the electrical resistance drops with increasing temperature because the hopping mobility increases with increasing thermal energy. Fig. 4b shows a completely opposite trend where resistance increases with temperature, a close resemblance to a bulk film, which is expected for a film

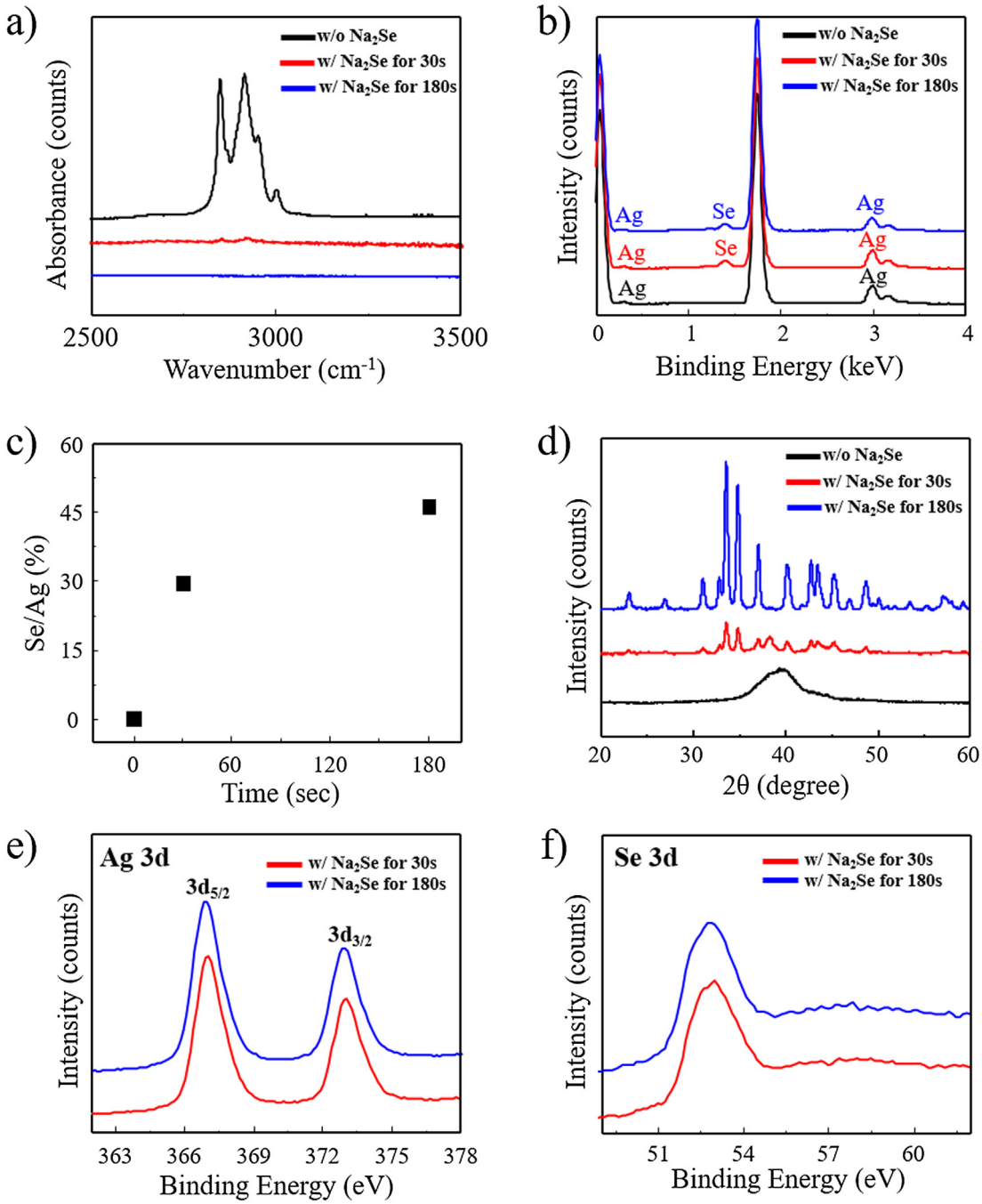

Fig. 2. (a) FTIR spectra (b) EDX map sum spectra of without Na_2Se (black), with Na_2Se for 30 s (red) and with Na_2Se for 180 s-treated Ag NCs thin-film. (c) Se: Ag ratio as a function of Na_2Se treating time measured by SEM-EDX. (d) XRD spectra of without Na_2Se (black), with Na_2Se for 30 s (red) and Na_2Se for 180 s-treated Ag NCs thin-film. XPS narrow scan analysis with Na_2Se for 30 s and 180 s treated Ag NCs thin films (e) Ag 3d spectrum and (f) Se 3d spectrum. (For interpretation of the references to colour in this figure legend, the reader is referred to the web version of this article.)

composed of fused and connected NCs. In a material exhibiting bulk-like transport, carrier mobility decreases with increasing temperature due to lattice scattering [57], which is observed here.

Lastly, we seek to understand why chemical transformation favorably occurs by Na_2Se treatment. In this process, the organic long carbon chain on Ag NCs are removed by Se^{2-} ion, and Se^{2-} ion subsequently diffused into the lattice of Ag NCs, forming a Ag_2Se thin film. Ag-Ag metallic bonding is weaker than Ag-Se ionic bonding [58], and thus Ag-Se bonding will be preferred. As the size of Ag NCs is very small (~4 nm) and has high surface energy, upon removal of surface stabilizing ligands, Ag NCs will tend to fuse with neighboring Ag NCs, creating enlarged Ag_2Se nanostructures. Indeed, a similar phenomenon was observed during the growth of Ag NCs upon the removal of surface ligands [59]. We believe that the high surface energy of small Ag NCs and high diffusivity of selenium atoms facilitate this chemical transformation.

Projecting toward the future, there is a high demand for wearable devices where robustness of the film under mechanical/temperature stress is of prime importance. Ag_2Se thin-film have a high potential for many flexible electronic applications, thus we conducted film mechanical strain and temperature stability test in this prospect. As shown in Fig. 5a, the gauge factor shows a linear increase for a constantly increasing strain from 0.2% up to 1% in both 30 s and 180 s Na_2Se treated films. The calculated gauge factor was around 3.6 and 0.8 at

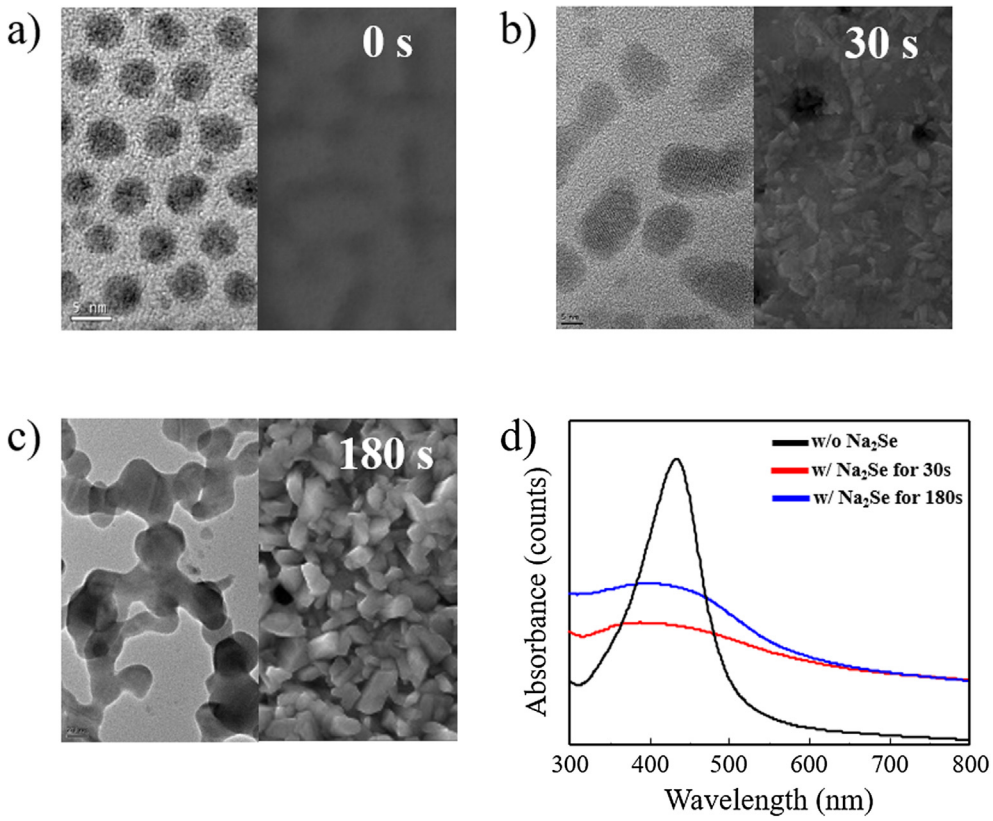

Fig. 3. TEM and SEM images of (a) without Na_2Se (b) with Na_2Se for 30 s (c) with Na_2Se for 180 s (d) UV–vis absorption spectra of without Na_2Se (black), with Na_2Se for 30 s (red) and Na_2Se for 180 s-treated Ag NCs thin-film. (For interpretation of the references to colour in this figure legend, the reader is referred to the web version of this article.)

strain values of up to 0.4% for 30 s and 180 s, respectively, and a slightly increase to 5.6 and 1.6 at a higher strain of 1.0% for 30 s and 180 s, respectively, were observed. Also, the thermal stability test of 180 s Na_2Se treated film is shown in Fig. 5b. The result demonstrates that after several heating/cooling cycles, Ag_2Se thin-film shows constant and reversible resistance changes from room temperature to 343 K. To demonstrate practical application as motion insensitive electrodes, we compared the 180 s Na_2Se treated Ag_2Se thin-film with conventional ligand exchanged (EDT) thin-film. Both thin-film placed on a human finger and resistance change was observed upon a bending motion of the finger, as shown in Fig. 5c and 5d. Ag_2Se thin-film did not show resistance *change upon bending of the finger while conventional ligand-exchanged thin-film* exhibited large resistance change upon bending. This results suggest that Ag_2Se thin-films can be advantageous when used as an electrode for wearable sensors.

4. Conclusions

In summary, we have demonstrate a single step, all solution-processed route to NCT using Ag NCs film as a starting materials platform. We have investigated a complete suite of material characterizations, including chemical, structural, optical, and electrical properties, of the transformation process. The final Ag_2Se film exhibited degenerately-doped n-type semiconductor with high carrier mobility. Film robustness toward mechanical strain and temperature cycling stress has also been examined. We believe that the NCT process demonstrated here is of wide applicability to other material systems which can open up new opportunities for solid-state chemist and device engineers.

CRediT authorship contribution statement

Md Ashraf Hossain: Conceptualization, Investigation, Validation,

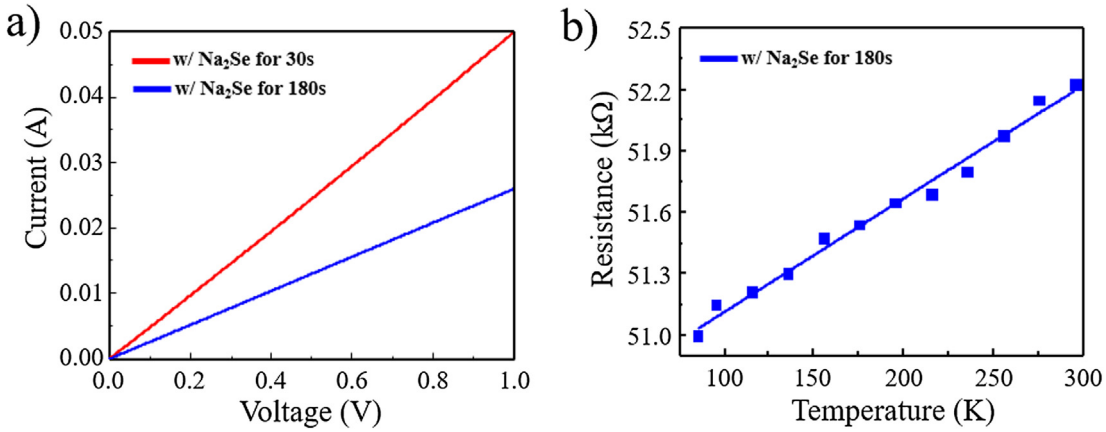

Fig. 4. (a) *I-V* characteristics curves of the 30 s (red) and 180 s (blue) Na_2Se-treated Ag NC thin-films (b) Charge-transport behavior of 180 s Na_2Se-treated Ag NCs thin-film. (For interpretation of the references to colour in this figure legend, the reader is referred to the web version of this article.)

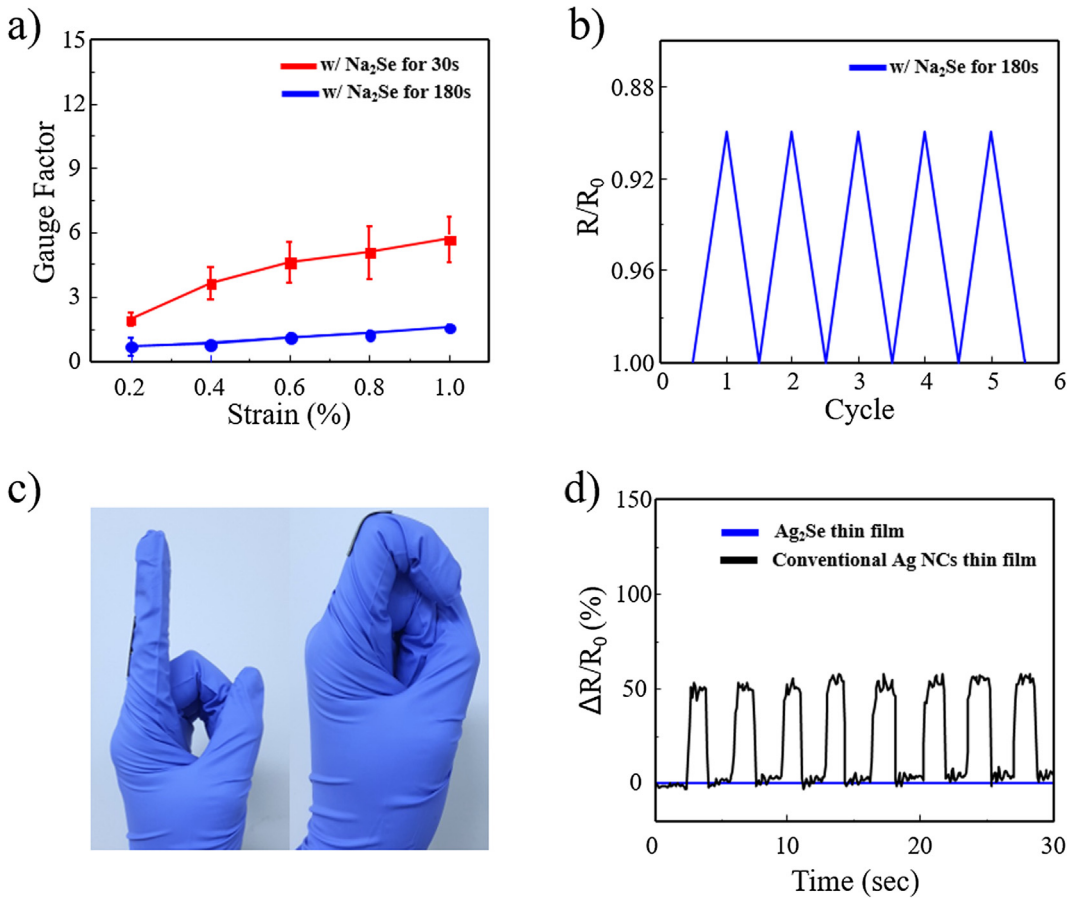

Fig. 5. (a) Gauge factor of Na_2Se-treared thin-film for 30 s (red) and 180 s (blue) as a function of mechanical strain. (b) Relative resistance changes in the 180 s Na_2Se-treated Ag NCs thin-film at room temperature to 343 K. (c) Images of a finger under straight and bending motion. (d) relative resistance changes in the Na_2Se-treated Ag NCs thin-film as function of a finger motion. (For interpretation of the references to colour in this figure legend, the reader is referred to the web version of this article.)

Writing - original draft. **Sanghyun Jeon:** Investigation, Validation. **Junhyuk Ahn:** Investigation, Validation. **Junsung Bang:** Investigation, Validation. **Ho Kun Woo:** Investigation, Validation. **Shihab B. Hafiz:** Investigation, Validation. **Dong-Kyun Ko:** Conceptualization, Funding acquisition, Writing - review & editing. **Soong Ju Oh:** Conceptualization, Supervision, Funding acquisition, Writing - review & editing.

Declaration of Competing Interest

The authors declare that they have no known competing financial interests or personal relationships that could have appeared to influence the work reported in this paper.

Acknowledgments

This research was supported by the Basic Science Research Program through the National Research Foundation of Korea (NRF) funded by the Ministry of Science, ICT and Future Planning (2019R1C1C1003319), Creative Materials Discovery Program through the National Research Foundation of Korea (NRF) funded by Ministry of Science, ICT and Future Planning (NRF-2018M3D1A1059001), and Korea University Future Research Grant. Shihab B. Hafiz gratefully acknowledges his graduate student support from US NSF (ECCS-1809112).

Appendix A. Supplementary material

Supplementary data to this article can be found online at https://doi.org/10.1016/j.apsusc.2020.145721.

References

[1] L. Carbone, C. Nobile, M. De Giorgi, F.D. Sala, G. Morello, P. Pompa, M. Hytch, E. Snoeck, A. Fiore, I.R. Franchini, M. Nadasan, A.F. Silvestre, L. Chiodo, S. Kudera, R. Cingolani, R. Krahne, L. Manna, Synthesis and micrometer-scale assembly of colloidal CdSe/CdS nanorods prepared by a seeded growth approach, Nano Lett. 7 (2007) 2942–2950.
[2] L.M. Moreau, C.A. Schurman, S. Kewalramani, M.M. Shahjamali, C.A. Mirkin, M.J. Bedzyk, How Ag nanospheres are transformed into AgAu nanocages, J. Am. Chem. Soc. 139 (2017) 12291–12298.
[3] G. Song, C. Liang, H. Gong, M. Li, X. Zheng, L. Cheng, K. Yang, X. Jiang, Z. Liu, Core-shell MnSe@Bi_2Se_3 fabricated via a cation exchange method as novel nanotheranostics for multimodal imaging and synergistic thermoradiotherapy, Adv. Mater. 27 (2015) 6110–6117.
[4] B.D. Anderson, J.B. Tracy, Nanoparticle conversion chemistry: kirkendall effect, galvanic exchange, and anion exchange, Nanoscale 6 (2014) 12195–12216.
[5] R. Panda, M. Panda, H. Rath, B.N. Dash, K. Asokan, U.P. Singh, R. Naik, N.C. Mishra, Structural and morphological modifications of $AgInSe_2$ and Ag_2Se composite thin films on 140 MeV Ni ion irradiation, Appl. Surf. Sci. 479 (2019) 997–1005.
[6] V. Krylova, S. Žalenkienė, N. Dukstienė, J. Baltrusaitis, Modification of polyamide-CdS-CdSe composite material films with Ag using a cation–cation exchange reaction, Appl. Surf. Sci. 351 (2015) 203–208.
[7] H.A. Atwater, A. Polman, Plasmonics for improved photovoltaic devices, Nat. Mater. 9 (2010) 205–213.
[8] C. Clavero, Plasmon-induced hot-electron generation at nanoparticle/metal-oxide interfaces for photovoltaic and photocatalytic devices, Nat. Photonics 8 (2014) 95.
[9] L. Hu, G. Chen, Analysis of optical absorption in silicon nanowire arrays for photovoltaic applications, Nano Lett. 7 (2007) 3249–3252.

[10] I.J. Peter, G. Vignesh, S. Vijaya, S. Anandan, K. Ramachandran, P. Nithiananthi, Enhancing the power conversion efficiency of $SrTiO_3$/CdS/Bi_2S_3 quantum dot based solar cell using phosphor, Appl. Surf. Sci. 494 (2019) 551–560.

[11] N. Liu, Z. Lu, J. Zhao, M.T. McDowell, H.-W. Lee, W. Zhao, Y. Cui, A pomegranate-inspired nanoscale design for large-volume-change lithium battery anodes, Nat. Nanotechnol. 9 (2014) 187.

[12] C. He, S. Wu, N. Zhao, C. Shi, E. Liu, J. Li, Carbon-encapsulated Fe_3O_4 nanoparticles as a high-rate lithium ion battery anode material, ACS Nano 7 (2013) 4459–4469.

[13] Z.-S. Wu, W. Ren, L. Wen, L. Gao, J. Zhao, Z. Chen, G. Zhou, F. Li, H.-M. Cheng, Graphene anchored with Co_3O_4 nanoparticles as anode of lithium ion batteries with enhanced reversible capacity and cyclic performance, ACS Nano 4 (2010) 3187–3194.

[14] F. Martinez-Julian, A. Guerrero, M. Haro, J. Bisquert, D. Bresser, E. Paillard, S. Passerini, G. Garcia-Belmonte, Probing lithiation kinetics of carbon-coated $ZnFe_2O_4$ nanoparticle battery anodes, J. Phys. Chem. C 118 (2014) 6069–6076.

[15] K. Ai, B. Zhang, L. Lu, Europium-based fluorescence nanoparticle sensor for rapid and ultrasensitive detection of an anthrax biomarker, Angew. Chem. Int. Ed. 121 (2009) 310–314.

[16] A. Yu, Z. Liang, J. Cho, F. Caruso, Nanostructured electrochemical sensor based on dense gold nanoparticle films, Nano Lett. 3 (2003) 1203–1207.

[17] I. Kim, K. Woo, Z. Zhong, P. Ko, Y. Jang, M. Jung, J. Jo, S. Kwon, S.-H. Lee, S. Lee, H. Youn, J. Moon, A photonic sintering derived Ag flake/nanoparticle-based highly sensitive stretchable strain sensor for human motion monitoring, Nanoscale 10 (2018) 7890–7897.

[18] N. Nath, A. Chilkoti, A colorimetric gold nanoparticle sensor to interrogate biomolecular interactions in real time on a surface, Anal. Chem. 74 (2002) 504–509.

[19] C. Cui, L. Gan, M. Heggen, S. Rudi, P. Strasser, Compositional segregation in shaped Pt alloy nanoparticles and their structural behaviour during electrocatalysis, Nat. Mater. 12 (2013) 765.

[20] L. Tian, X. Yan, X. Chen, Electrochemical activity of iron phosphide nanoparticles in hydrogen evolution reaction, ACS Catal. 6 (2016) 5441–5448.

[21] M.-H. Shao, K. Sasaki, R.R. Adzic, Pd−Fe nanoparticles as electrocatalysts for oxygen reduction, J. Am. Chem. Soc. 128 (2006) 3526–3527.

[22] S. Choi, H. Lee, R. Ghaffari, T. Hyeon, D.-H. Kim, Recent advances in flexible and stretchable bio-electronic devices integrated with nanomaterials, Adv. Mater. 28 (2016) 4203–4218.

[23] M. Su, F. Li, S. Chen, Z. Huang, M. Qin, W. Li, X. Zhang, Y. Song, Nanoparticle based curve arrays for multirecognition flexible electronics, Adv. Mater. 28 (2016) 1369–1374.

[24] N. Ahammed, L.G. Asirvatham, S. Wongwises, Thermoelectric cooling of electronic devices with nanofluid in a multiport minichannel heat exchanger, Exp. Therm. Fluid Sci. 74 (2016) 81–90.

[25] J.H. Kim, J.G. Kim, J. Song, T.-S. Bae, K.-H. Kim, Y.-S. Lee, Y. Pang, K.H. Oh, H.-S. Chung, Investigation of the growth and in situ heating transmission electron microscopy analysis of Ag_2S-catalyzed ZnS nanowires, Appl. Surf. Sci. 436 (2018) 556–561.

[26] P.T. Yin, S. Shah, M. Chhowalla, K.-B. Lee, Design, synthesis, and characterization of graphene-nanoparticle hybrid materials for bioapplications, Chem. Rev. 115 (2015) 2483–2531.

[27] X. Guo, Z. Wu, W. Li, Z. Wang, Q. Li, F. Kong, H. Zhang, X. Zhu, Y.P. Du, Y. Jin, Y. Du, J. You, Appropriate size of magnetic nanoparticles for various bioapplications in cancer diagnostics and therapy, ACS Appl. Mater. Interfaces 8 (2016) 3092–3106.

[28] F. Li, J. Lu, X. Kong, T. Hyeon, D. Ling, Dynamic nanoparticle assemblies for biomedical applications, Adv. Mater. 29 (2017) 1605897.

[29] X. Cheng, J. Liu, X. Wan, H. Wang, Y. Li, J. Liu, H. Rong, M. Xu, W. Chen, J. Zhang, Phosphine ligand-mediated kinetics manipulation of aqueous cation exchange: a case study on the synthesis of Au@SnSx core–shell nanocrystals for photoelectrochemical water splitting, Chem. Commun. 54 (2018) 9993–9996.

[30] D. Zhang, A.B. Wong, Y. Yu, S. Brittman, J. Sun, A. Fu, B. Beberwyck, A.P. Alivisatos, P. Yang, Phase-selective cation-exchange chemistry in sulfide nanowire systems, J. Am. Chem. Soc. 136 (2014) 17430–17433.

[31] J. Feng, J. Liu, X. Cheng, J. Liu, M. Xu, J. Zhang, Hydrothermal cation exchange enabled gradual evolution of Au@ZnS–AgAuS yolk-shell nanocrystals and their visible light photocatalytic applications, Adv. Sci. 5 (2018) 1700376.

[32] L. Liu, P. Hu, Y. Li, W. An, J. Lu, W. Cui, P_3HT-coated Ag_3PO_4 core-shell structure for enhanced photocatalysis under visible light irradiation, Appl. Surf. Sci. 466 (2019) 928–936.

[33] J.L. Fenton, R.E. Schaak, Structure-selective cation exchange in the synthesis of zincblende MnS and CoS nanocrystals, Angew. Chem. Int. Ed. 56 (2017) 6464–6467J.

[34] H. Li, M. Zanella, A. Genovese, M. Povia, A. Falqui, C. Giannini, L. Manna, Sequential cation exchange in nanocrystals: preservation of crystal phase and formation of metastable phases, Nano Lett. 11 (2011) 4964–4970.

[35] Q. Zhang, L. Gao, Synthesis of nanocrystalline aluminum nitride by nitridation of δ-Al_2O_3 nanoparticles in flowing ammonia, J. Am. Ceram. Soc. 89 (2006) 415–421.

[36] J. Park, H. Zheng, Y.-W. Jun, A.P. Alivisatos, Hetero-epitaxial anion exchange yields single-crystalline hollow nanoparticles, J. Am. Chem. Soc. 131 (2009) 13943–13945.

[37] H. Zhang, L.V. Solomon, D.-H. Ha, S. Honrao, R.G. Hennig, R.D. Robinson, (NH4) 2S, a highly reactive molecular precursor for low temperature anion exchange reactions in nanoparticles, Dalton Trans 42 (2013) 12596–12599.

[38] J. Zhang, W. Wu, C. Zhang, Z. Ren, X. Qian, Prussian-blue analog-derived Co_3S_4/MoS_2 porous nanocubes as enhanced Pt-free electrode catalysts for high-efficiency dye-sensitized solar cells, Appl. Surf. Sci. 484 (2019) 1111–1117.

[39] D.T. Schoen, C. Xie, Y. Cui, Electrical switching and phase transformation in silver selenide nanowires, J. Am. Chem. Soc. 129 (2007) 4116–4117.

[40] Y. Ding, Y. Qiu, K. Cai, Q. Yao, S. Chen, L. Chen, J. He, High performance n-type Ag2Se film on nylon membrane for flexible thermoelectric power generator, Nat. Commun. 10 (2019) 841.

[41] A. Shrestha, M. Batmunkh, C.J. Shearer, Y. Yin, G.G. Andersson, J.G. Shapter, S. Qiao, S. Dai, Nitrogen-doped CNx/CNTs heteroelectrocatalysts for highly efficient dye-sensitized solar cells, Adv. Energy Mater. 7 (2017) 1602276.

[42] S.B. Hafiz, M.R. Scimeca, P. Zhao, I.J. Paredes, A. Sahu, D.-K. Ko, Silver selenide colloidal quantum dots for mid-wavelength infrared photodetection, ACS Appl. Nano Mater. 2 (2019) 1631–1636.

[43] S.B. Hafiz, M. Scimeca, A. Sahu, D.-K. Ko, Colloidal quantum dots for thermal infrared sensing and imaging, Nano Convergence 6 (2019) 7.

[44] M.R. Scimeca, S.B. Hafiz, A. Sahu, D.-K. Ko, Mid-Infrared Colloidal Quantum Dot Based Nanoelectronics and Nanooptoelectronics, ECS Trans. 92 (2019) 11–16.

[45] J. Yuan, P. Wang, C. Hao, G. Yu, Photoelectrochemical reduction of carbon dioxide at $CuInS_2$/graphene hybrid thin film electrode, Electrochim. Acta 193 (2016) 1–6.

[46] K. Shao, Y. Wang, M. Iqbal, L. Lin, K. Wang, X. Zhang, M. He, T. He, Modification of Ag nanoparticles on the surface of $SrTiO_3$ particles and resultant influence on photoreduction of CO_2, Appl. Surf. Sci. 434 (2018) 717–724.

[47] W. Wang, Y. Geng, Y. Qian, M. Ji, Y. Xie, A novel room temperature method to nanocrystalline Ag_2Se, Mater. Res. Bull. 34 (1999) 877–882.

[48] G. Sáfrán, O. Geszti, G. Radnóczi, P.B. Barna, TEM study of Ag_2Se developed by the reaction of polycrystalline silver films and selenium, Thin Solid Films 317 (1998) 72–76.

[49] G. Henshaw, I.P. Parkin, G.A. Shaw, Convenient, room-temperature liquid ammonia routes to metal chalcogenides J. Chem. Soc., Dalton Trans., (1997) 231–236.

[50] J. Qu, N. Goubet, C. Livache, B. Martinez, D. Amelot, C. Gréboval, A. Chu, J. Ramade, H. Cruguel, S. Ithurria, M.G. Silly, E. Lhuillier, Intraband mid-infrared transitions in Ag_2Se nanocrystals: potential and limitations for Hg-free low-cost photodetection, J. Phy. Chem. C 122 (2018) 18161–18167.

[51] P.P.J. Helan, K. Mohanraj, G. Sivakumar, Synthesis and characterization of β-Ag2Se and β-AgCuSe nanoparticles via facile precipitation route, Trans. Nonferrous Met. Soc. China 25 (2015) 2241–2246.

[52] M.A. Hossain, S. Jeon, J. Ahn, H. Joh, J. Bang, S.J. Oh, Control of tunneling gap between nanocrystals by introduction of solution processed interfacial layers for wearable sensor applications, J. Ind. Eng. Chem. 73 (2019) 214–220.

[53] J.-P. Ge, S. Xu, L.-P. Liu, Y.-D. Li, A Positive-microemulsion method for preparing nearly uniform Ag2Se nanoparticles at low temperature, Chem.–Eur. J. 12 (2006) 3672–3677.

[54] H. Oh, S.-W. Lee, M. Kim, W.S. Lee, M. Seong, H. Joh, M.G. Allen, G.S. May, M.S. Bakir, S.J. Oh, Designing surface chemistry of silver nanocrystals for radio frequency circuit applications, ACS Appl. Mater. Interface 10 (2018) 37643–37650.

[55] J.A. Faucheaux, A.L.D. Stanton, P.K. Jain, Plasmon resonances of semiconductor nanocrystals: physical principles and new opportunities, J. Phys. Chem. Lett. 5 (2014) 976–985.

[56] P.-W. Chiu, M. Kaempgen, S. Roth, Band-structure modulation in carbon nanotube T junctions, Phys. Rev. Lett. 92 (2004) 246802.

[57] R.F. Pirret, Semiconductor Device Fundamentals.second ed.., Addison Wesley Longman.

[58] A. Bergqvist, M. Drechsler, O. De Jong, S.-N.C. Rundgren, Representations of chemical bonding models in school textbooks – help or hindrance for understanding? Chem. Educ. Res. Pract. 14 (2013) 589–606.

[59] H. Joh, W.S. Lee, M.S. Kang, M. Seong, H. Kim, J. Bang, S.-W. Lee, M.A. Hossain, S.J. Oh, Surface design of nanocrystals for high-performance multifunctional sensors in wearable and attachable electronics, Chem. Mater. 31 (2019) 436–444.